How Cells Feel: Stochastic Model for a Molecular Mechanosensor

Matteo Escudé, Michelle K. Rigozzi, and Eugene M. Terentjev*
Cavendish Laboratory, University of Cambridge, Cambridge, United Kingdom

ABSTRACT Understanding mechanosensitivity (i.e., how cells sense the stiffness of their environment) is very important, yet there is a fundamental difficulty in understanding its mechanism: to measure an elastic modulus one requires two points of application of force—a measuring and a reference point. The cell in contact with substrate has only one (adhesion) point to work with, and thus a new method of measurement needs to be invented. The aim of this theoretical work is to develop a self-consistent physical model for mechanosensitivity, a process by which a cell detects the mechanical stiffness of its environment (e.g., a substrate it is attached to via adhesion points) and generates an appropriate chemical signaling to remodel itself in response to this environment. The model uses the molecular mechanosensing complex of latent TGF-β attached to the adhesion point as the biomarker. We show that the underlying Brownian motion in the substrate is the reference element in the measuring process. The model produces a closed expression for the rate of release of active TGF-β, which depends on the substrate stiffness and the pulling force coming from the cell in a subtle and nontrivial way. It is consistent with basic experimental data showing an increase in signal for stiffer substrates and higher pulling forces. In addition, we find that for each cell there is a range of stiffness where a homeostatic configuration of the cell can be achieved, outside of which the cell either relaxes its cytoskeletal forces and detaches from the very weak substrate, or generates an increasingly strong pulling force through stress fibers with a positive feedback loop on very stiff substrates. In this way, the theory offers the underlying mechanism for the myofibroblast conversion in wound healing and smooth muscle cell dysfunction in cardiac disease.

INTRODUCTION

Complex living organisms are made of trillions of cells that constantly grow, interact, and reproduce, each one of them performing specific and fundamental tasks for life. Scientists have always been fascinated by how each one of them appears to be aware of its role and able to interact with its surroundings as if they possessed true sensory organs. The general question we seek to answer in this work is: how do cells feel the mechanical stiffness of their environment? Through the application of a classical physical model of coupled stochastic processes, we expand our understanding of the sensory activity of cells.

A large amount of research has been devoted to studying the mechanisms behind chemical signal detection at the cellular level, a sensory activity that could be compared to the olfactory ability of animals and humans. However, in the last two decades there has been growing evidence that cells are not only receptive to the concentration of chemicals in their environment, but also to mechanical properties of objects they are in contact with. These mechanical properties include viscosity, hydrostatic pressure, and deformability, as well as topographic profiles: features of materials that animals perceive through complex tactile organs. To provide concrete examples: cellular cytoskeletal changes (1–3), adhesions (4), contractile forces (5), stiffness (2), and migration (4) have all been shown to be affected by the mechanical properties of the substrate the cell is attached to. Cellular differentiation, based on changes in substrate stiffness, is another emblematic area where mechanosensitivity is observed. Notable evidence for this includes the work by Engler et al. (6) on how stem cell lineage is specified by matrix elasticity. A similar example, which is a more specific focus of this article, is the process of differentiation of fibroblasts into myofibroblasts as a response to a stiffer substrate. A most remarkable biological investigation of this system has been carried out by Wipff et al. (7).

Mechanosensing is defined as when at least one chemical reaction in the cell changes characteristics in response to a change in its mechanical environment. We specifically wish to distinguish from a very different case when external forces are applied to the cell. There is a lot of research on that problem, but ultimately it has no mystery: there are many molecular processes that respond to an applied force and probably several different ones are employed by cells in different situations. It is much more challenging to understand how cells could detect the stiffness of a passive matrix they are in contact with. Such a sensor requires a mechanical structure with the ability to produce changes in a chemical signal, which are in turn detectable by receptors in the cell. The sensor specifically investigated in this work is the latent complex of the transforming growth factor-β (latent TGF-β): a large biomolecular complex that has been shown to be associated with smooth-muscle actin expression (8) and, in particular, to have the stretch-sensing features that cause the embryonic-stem-cell-to-smooth-muscle-cell (9) or the fibroblast-to-myofibroblast differentiation (7).

Submitted August 15, 2013, and accepted for publication October 28, 2013.

*Correspondence: emt1000@cam.ac.uk

Matteo Escudé and Michelle K. Rigozzi contributed equally to this work.

Editor: Cecile Sykes.

0006-3495/14/01/0124/10 $2.00

http://dx.doi.org/10.1016/j.bpj.2013.10.042

We defer the biological details to the next section. What is specifically relevant to the basic physical picture is the fact that a passive biomolecular complex is able to perform a measurement of stiffness on its environment. When humans wish to detect the stiffness of an object, with machinery or with their tactile organs, they usually perform two separate measurements: force (or stress); and displacement (or strain). The measure of stiffness is obtained by a ratio relating these two physical parameters. What is crucial to this kind of measurement is that the apparatus requires two points of application: to measure displacement a fixed reference point is always needed; to measure force one has to ensure a reference point as well. We need two fingers to squeeze a test object from two sides—or use just one finger for measurement of an object against a reliably fixed wall. In the same way, all engineered devices ultimately have two points of application on the test sample. A simple sensor like the latent TGF-β complex, which is effectively a molecular protuberance outside the cell surface, does not possess these features: it only has one finger (or point of application) through which a pulling force is transmitted from the cell interior and no a priori information about the reference point in the substrate, so how can it perform this measurement? This is the question driving our work.

As a result of this work, we conclude that the measuring process is carried out thanks to the microscopic thermal fluctuations (Brownian motion) of the sensor and of the substrate, which result in a different statistical behavior in environments with different stiffness. The biomolecular measuring complex has evolved so that its characteristic energy scale is comparable to that of thermal fluctuation in the typical cell environment, allowing the small cellular forces to affect the statistics of latent complex rupture.

Other physical models have been developed in this field, notably that of Schwarz et al. (10). They have proposed a model that is meant to describe the mechanosensing activity of focal adhesions. Specifically, they introduce a two-spring model where the extracellular and intracellular mechanical environments are described as two springs in series connected by a breakable bond: a construction very similar to what we shall be employing below. However, in keeping with the established methods, they assume that the cell imposes a force-dependent velocity $v(F)$ on the first spring, while the far end of the second spring remains fixed. This makes the whole problem dynamic and the fundamental difficulty of a mechanical measurement with just one point of application is no longer present: there is never a state of mechanical equilibrium along the series of springs. The force-dependent rate of rupture is then written by using the phenomenological expression of Bell,

$$k(F) = k_0 e^{Fx_0/k_B T},$$

where k_0 is the rate of rupture without force applied and x_0 is the characteristic length scale describing the free energy of the bond (11). Of course, the Bell formula has been originally derived by Kramers (12), in extending his classical solution for the equilibrium rate of escape over an energy barrier to when an external force modifies the potential energy: $V(x) - Fx$. These ideas were extensively used by Dudko et al. (13) in the context of single-molecule pulling experiments.

There are a number of elegant experiments that demonstrate the constant nature of the force exerted by the cell (14–16). Compared to Schwarz et al. (10), we offer a more fundamental explanation of the physical phenomenon because it draws on the principles of statistical mechanics rather than on a phenomenological observation, and also observes the mechanical balance laws. Our work also provides an improvement to the model of Dudko et al. (13) because approaching the critical breakdown force, our expression for the rate of escape shows the correct diverging behavior. The final result we obtain has the Bell formula in the high barrier limit embedded in it; however, other factors critically involving the stiffness of the substrate dominate the behavior.

THE BIOLOGICAL SYSTEM

The specific stretch-sensor, based on the latent complex of TGF-β, has been selected because it is expected to be representative of a broader family of mechanosensors and also because of the abundance of biophysical research providing reliable evidence of its behavior. In this account of the biological system, we primarily follow the works of Sinha et al. (1), Wipff et al. (7), and Tomasek et al. (17).

Fibroblasts are the most common type of cell in connective tissue, and among other functions, are crucial to the process of physiological tissue repair. Specifically, when a wound is formed, fibroblasts differentiate into myofibroblast, a highly contractile form that helps to pull the wound together and facilitates the healing process. The highly contractile state of the myofibroblasts is generated by α-smooth muscle actin (α-SMA) in stress fibers, appearance of which marks the transition between the two states. In a very similar way, smooth muscle cells of arterial wall stiffen by overexpression of α-SMA when a rigid crystalline plaque forms underneath them in the arterial cavity. In both cases, the release of TGF-β has been unambiguously registered (7,8).

The differentiation of fibroblasts into myofibroblasts has been shown to be reproducible in vitro by plating fibroblasts on substrates with different stiffness. For substrates stiffer than a specific Young modulus, $E \gtrsim 11$ kPa (7), fibroblasts differentiate into myofibroblasts. If plated on a softer substrate ($E << 11$ kPa), however, fibroblasts do not transform and remain in the fibroblast state—and myofibroblasts turn back into fibroblasts. The value of ~10 kPa is particularly interesting because it is similar to the difference in stiffness between wound tissue and typical connective tissue (18).

Strong evidence suggests that this phenotype change is caused by the mechanical activation of latent TGF-β as a biomarker (19). When active TGF-β is released into the cell surroundings, it can bind to specific receptors on the cell surface, and the cell is induced to synthesize three types of protein crucial to the signaling loop, namely more of the latent TGF-β complex, α-SMA, and matrix proteins (7,20). The latent complex is produced to add to the body of sensors, some of which have been broken, and the α-SMA forms more contractile fibers in the cell, increasing the force applied to the latent complex molecules. Hinz et al. (20) specifically confirm that an increased α-SMA expression is sufficient to enhance fibroblast contractile activity. The latent complex adheres to integrins on the cell surface which, intracellularly, are bound to the contractile cytoskeleton. Outside the cell, the latent complex is attached to the extracellular matrix via proteins such as fibronectin (21) (Fig. 1). When the cell contracts, the latent complex is put under tension. However, we have to question the beautiful and intuitively clear picture proposed by Wipff et al. (7) and Wells and Discher (22): since the cell exerts a (constant) force, it does not matter whether the substrate deforms (in the soft case) or stays rigid—basic mechanics tells that in all cases the tension remains constant along the chain of elements in Fig. 1. If one wants to relate the rate of active TGF-β release to the force applied to the latent complex, e.g., by Bell's formula, as in Schwarz et al. (10)—this cannot be different between the soft and stiff cases. Resolving this problem is our aim here.

THE MODEL

No analytical theory for the mechanosensing role of TGF-β exists in the literature. Our model is inspired by the two-spring construction of Schwarz et al. (10) and is illustrated in Fig. 2. We treat the substrate (which could be either the extracellular matrix or an artificial material) as a one-dimensional viscoelastic Voigt system: the effective spring attached to a distant fixed point is characterized by two parameters, an effective spring constant κ, representing its elastic modulus; and a damping coefficient, γ_1. It is important to distinguish this from a commonly used Maxwell model for viscoelasticity of polymer melts and complex fluids: although the relaxation time is the same, only with an elastic and a dissipative element in parallel can one model a gel with an equilibrium elastic modulus.

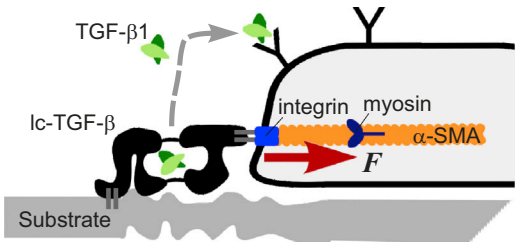

FIGURE 1 Illustration of the biological system: the cell attachment to a deformable substrate, the application of pulling force F, and the release of active TGF-β. On binding to a receptor on the cell surface, TGF-β initiates two processes: production of the new latent complexes (to replenish the broken ones) and of the smooth-muscle actin (to stiffen the stress fibers and increase the pulling). Although this image is frequently found in the literature, it is not often appreciated that the force acting on the latent complex is always F irrespective of how much the substrate is deformed. To see this figure in color, go online.

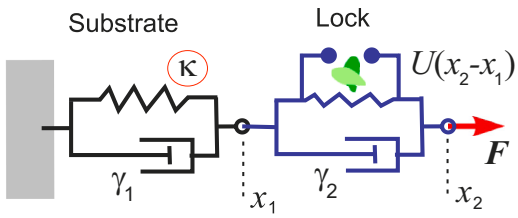

FIGURE 2 The lock, representing the latent TGF-β complex, is pulled by the cell with a constant force F and is coupled to a viscoelastic substrate with the equilibrium stiffness κ. Both elements have a dissipative (friction) component to their response, described by the constants γ_1 and γ_2, respectively. The positions of the substrate and lock deviation of equilibrium are x_1 and x_2. To see this figure in color, go online.

This viscoelastic spring is connected in series with the latent complex of TGF-β, which in turn is connected to the rigid integrin complex in the cell that applies a constant pulling force F to the system. An assumption of constant local force F exerted by the cell is adopted because for the timescales relevant to thermally driven escape, the force may be assumed time-independent. Any change in pulling force by the cell is caused by the chemical signaling loop, which is dependent on diffusion distances much larger than the ones characterizing the model.

The latent TGF-β is modeled by a lock, which could break if it gains enough thermal energy to escape a barrier given by a potential $U(x)$, meaning the subsequent rupture of the complex and release of the small molecule responsible for the signal: the active TGF-β. The sketch in Fig. 2 shows that it is the relative displacement of the two ends $(x_2 - x_1)$ that is the correct argument of the potential. The damping properties of the lock are described by a coefficient γ_2, in the same way as with the viscoelastic spring for the substrate. Both the lock and the substrate are subject to distinct stochastic forces, satisfying their separate fluctuation-dissipation relations, which (the thermal motion) is the key element to the whole process. We write and solve a set of coupled stochastic differential equations that describe the system to find the rate of escape over such a barrier. This is the rate at which active TGF-β is released, initiating the signaling loop that will ultimately cause, e.g., the overexpression of α-actin resulting in the fibroblast conversion to myofibroblast, or the stiffening of smooth muscle cells.

To write the master kinetic equation for the system we shall follow a route similar to the one taken by Graham

(23), because it provides a concise and rigorous method to derive the Fokker-Planck equation from a set of coupled overdamped Langevin equations:

$$\gamma_1 \dot{x}_1 = -\kappa x_1 + \frac{dU}{d(x_2 - x_1)} + \sqrt{2k_B T\,\gamma_1} \cdot \zeta_1(t), \quad (1)$$

$$\gamma_2 \dot{x}_2 = -\frac{dU}{d(x_2 - x_1)} + F + \sqrt{2k_B T\,\gamma_2} \cdot \zeta_2(t). \quad (2)$$

Here the base stochastic process $\zeta_i(t)$ is assumed to be Gaussian and normalized to unity. Note that it is the difference in independent position coordinates $x_2 - x_1$ that affects the lock. The steps of derivation are standard, and as a result we obtain the Cartesian components of diffusion current in the space of $\{x_2 - x_1\}$,

$$J_i = -\frac{k_B T}{\gamma_i} e^{-V_{\text{eff}}/k_B T} \frac{\partial}{\partial x_i}\left(e^{V_{\text{eff}}/k_B T} P\right) \quad i = 1, 2, \quad (3)$$

where

$$V_{\text{eff}}(x_1, x_2) = \frac{1}{2}\kappa x_1^2 - F x_2 + U(x_2 - x_1)$$

represents the effective potential landscape over which the substrate and the latex complex move, subject to thermal excitation. The components J_1 and J_2 naturally have different diffusion constants: $k_B T/\gamma_1$ and $k_B T/\gamma_2$, respectively. This issue is addressed by changing variables,

$$x_1 \to \sqrt{\gamma_2/\gamma_1}\tilde{x}_1,\ x_2 \to \sqrt{\gamma_1/\gamma_2}\tilde{x}_2,$$

giving the unique diffusion coefficient

$$\tilde{D} = k_B T/\sqrt{\gamma_1 \gamma_2}$$

in the transformed Eq. 3. We now have an expression for the vector current in two dimensions and can apply the Kramers theory of escape over a potential barrier, following the original work (12) and the analysis by Chandrasekhar (24). Interested readers may obtain additional technical details in the Supporting Material.

THE POTENTIAL LANDSCAPE

To study the effective potential landscape it is most convenient to transform the coordinates, replacing the second variable x_2 with the net separation $u = x_2 - x_1$, which is the natural variable of the lock potential $U(u)$. To be specific, it is useful to express $U(u)$ in an explicit functional form. Following Dudko et al. (13), we use a cubic function, which gives a realistic profile to the barrier and naturally excludes the possibility of rebinding by falling to negative infinity for large u. It is tuned so that the minimum is at $u = 0$ and the maximum of height Δ is at $u = u_0$:

$$U(u) = \frac{3}{2}\Delta\left(\frac{u}{u_0} - \frac{1}{2}\right) - 2\Delta\left(\frac{u}{u_0} - \frac{1}{2}\right)^3 + \frac{\Delta}{2}. \quad (4)$$

Substituting this into $V_{\text{eff}}(x_1,u)$, the potential landscape may be readily plotted, for instance at constant $x_1 = 0$ (i.e., nondeformed substrate), to study how the landscape evolves for different values of force F and elastic constant κ (Fig. 3 *a*). Contour plots of the effective potential as a map on (x_1,u) plane provide a useful tool for finding the optimal path of the system evolution (Fig. 3 *b*).

We now proceed to analyze the potential surface more rigorously by finding the position of the extrema and the values of $V_{\text{eff}}(x_1,u)$ at those points. By calculating the derivatives of the function, one finds the potential has two extrema (points A and C in Fig. 3):

$$x_1(A) = \frac{F}{\kappa},\ u(A,C) = \frac{1}{2}u_0\left(1 \mp \sqrt{1 - \frac{2}{3}\frac{F u_0}{\Delta}}\right),$$
$$V_{\text{eff}}(A) \approx -\frac{F^2}{2\kappa} - \frac{F^2 u_0^2}{12\Delta},\ \Delta V = \frac{\Delta(3 - 2F u_0/\Delta)^{3/2}}{3\sqrt{3}}. \quad (5)$$

The bottom of the well (A) and the saddle point (C) have the same x_1 coordinate. For $F_C = 3\Delta/2u_0$, the two extrema coincide and the path from the origin to the bottom of the potential landscape has no energy barrier: the system shown in Fig. 2 breaks down. This effective barrier has to be overcome by the substrate-and-lock system as it evolves

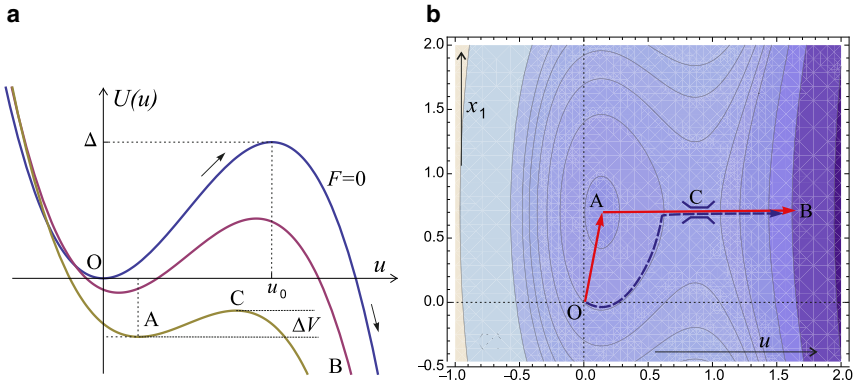

FIGURE 3 (*a*) Plot of the cubic function describing V_{eff} at $x_1 = 0$, the bottom of the well at $u = 0$, and the top of the energy barrier of height Δ at $u = u_0$. (*Dashed lines*) Increasing applied force F, labeled on plot. (*b*) Contour plot of $V_{\text{eff}}(x_1,u)$. (*Darker areas*) Lower energy values. In this plot we have chosen the values of $\tilde{\kappa} = \kappa u_0^2/\Delta = 0.4$ and $\tilde{f} = F u_0/\Delta = 0.3$. The latter value corresponds to the 0.2 of the critical force F_C. (*Solid arrows*) Approximation used to the preferred path $O \to A \to C \to B$ along the potential surface; (*dashed line*) example of another path, with lower potential barrier but an effectively much lower rate. To see this figure in color, go online.

under thermal fluctuations. The important point in this potential landscape analysis is that the barrier height $\Delta V = V_{\text{eff}}(C) - V_{\text{eff}}(A)$ does not depend on the substrate stiffness, while the depth of the potential well (A) does include the constant factor $-\beta F^2/2\kappa$.

THE RATE EXPRESSION

Applying the Kramers theory to generalized problems of thermally activated diffusion over a potential barrier is a relatively standard operation (25) and we are not going to go into details. There have been more recent articles on the calculation of escape rate in two dimensions (26,27), which often are variations the original treatment by Langer (28). However, there are two important new, to our knowledge, steps that we make, which will be discussed here (see the Supporting Material for technical details).

To begin, we want to be able to have solutions for any value of external applied force F, including near the critical breakdown point F_C. The standard approach, e.g., that of Dudko et al. (13) and Yohichi and Dudko (26), is to remain in the limit of weak forces ($F << \Delta/u_0$ in our notation) where the required integration over the potential barrier,

$$\int_A^B \exp\left[V_{\text{eff}}(u)/k_{\text{B}}T\right]du,$$

can be accurately approximated by the saddle-point expression at point (C). However, this approximation fails as the barrier height ΔV diminishes to zero and the predicted reaction rate no longer describes the correct physical process of free escape. We use a different method, essentially approximating the whole exponential (as opposed to the exponent) by a parabola pinned to the correct values of V_{eff} at (A) and (C) and integrate only from A to C, doubling the value of the integral afterwards. This method accurately describes the result near the critical breakdown point ($A \to C$), and retains the correct activation exponential factor at smaller forces. In effect, this method makes the same-magnitude error in evaluating the integral, but retains the accuracy near the critical force point. As a result, the steady-state flux of escape over the barrier (C) takes the form

$$J \approx \frac{3}{2}\frac{\tilde{D}}{(u_C - u_A)(1 + 2e^{\Delta V/k_{\text{B}}T})} \cdot P(A), \qquad (6)$$

where u_C, u_A, and ΔV (all functions of F) are given in the expressions in Eq. 5 and $P(A)$ is the probability for the system to reach the bottom of the potential well (A).

The next point of novelty is related to the evaluation of the number of particles available at (A), N_A, that is, before the barrier—so that the rate of the escape over the barrier is given by the ratio $k = J/N_A$ (as is standard in the Kramers problem). This number is given by the integral around this potential minimum:

$$N_A = \int P(A)\exp\left[-V_{\text{eff}}/k_{\text{B}}T\right]\text{d}l.$$

Because we are on a two-dimensional plane, the path of this integration is not straight on the (x_1,u) plane. The path is marked on the landscape map in Fig. 3 *b* and the curvature of energy surface is not the same in the x_1- and u-directions around the minimum at (A). On the first leg, when the system is sinking down the potential well ($O \to A$), the curvature is κ, the elastic modulus of the substrate, whereas on the second leg, when the system is approaching the saddle ($A \to C$), the curvature is

$$6\left(\Delta/u_0^2\right)\sqrt{1 - 2Fu_0/3\Delta}.$$

Therefore the overall result for the number of particles is determined by the weighted mean of the two curvatures (due to the Gaussian nature of the integral), giving

$$N_A \approx \sqrt{2\pi k_{\text{B}}T}\,\frac{F + \kappa u_0\sqrt{1 - 2Fu_0/3\Delta}}{3\kappa(2\Delta/u_0 - F)}\,e^{F^2/2\kappa k_{\text{B}}T}P(A). \quad (7)$$

Note that the dependence on external pulling force F is prominent in the expression for the flux over the barrier, Eq. 6, entering via ($u_C - u_A$) and ΔV—both shown in the expressions in Eq. 5. In contrast, it is the statistical weight of the system at the bottom of the deformed potential well, Eq. 7, where a strong dependence on the substrate elasticity κ appears. The resulting expression for the rate of escape (the rupture of the latent TGF-β complex, in our context) is given by the ratio of the two expressions (Eqs. 6 and 7), $k = J/N_A$; it is quite a complicated and cumbersome formula. Here, for simplicity and clarity, we only plot the rate dependence on the substrate stiffness and also examine two relevant limiting cases.

To be able to plot functions in nondimensional form, we need to establish the relevant scales. Let us compare the applied force to the strength of the original lock potential $U(u)$, and assume that in most cases the force is weaker than the native latent complex (i.e., does not break it outright): this means small $\tilde{f} = Fu_0/\Delta$. Let us also compare the stiffness of the substrate to the stiffness of the original lock, that is, measure $\tilde{\kappa} = \kappa u_0^2/\Delta$. We must always assume that the original latent complex is stable at the typical temperature, that is, $\Delta/k_{\text{B}}T$ is large.

We begin by studying how the rate varies with different substrate stiffness, which was indeed the reason that stimulated this research in the first instance. Plotting the rate as a function of κ (Fig. 4), we observe that for any pulling force on stiffer substrates, the latent complex is more likely to rupture, confirming the phenomenological interpretation discussed in the literature reviewed above. The functional form for the rate also appears to flatten considerably when κ is greater than a certain threshold

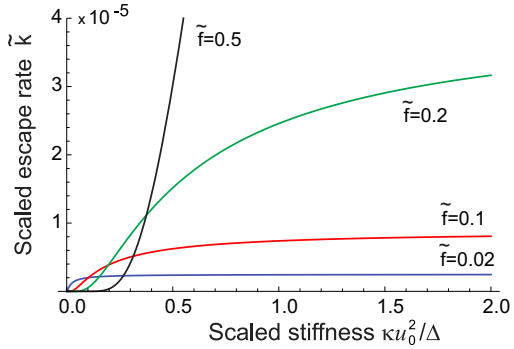

FIGURE 4 The rate of latent complex rupture (and active TGF-β escape), scaled in nondimensional units as $\tilde{k} = k \cdot 2\sqrt{2\pi}u_0^3/9\sqrt{k_B T D}$, plotted as function of substrate stiffness κ (also scaled in nondimensional units, see text). The curves are for different values of scaled force, $\tilde{f} = Fu_0/\Delta$, labeled on the plot. As the pulling force increases, the region of steepest response of the mechanosensing complex to the substrate stiffness shifts toward higher stiffness, and also becomes more diffuse—enabling a graded response, as opposed to a very sharp response at small forces on very soft substrates. To see this figure in color, go online.

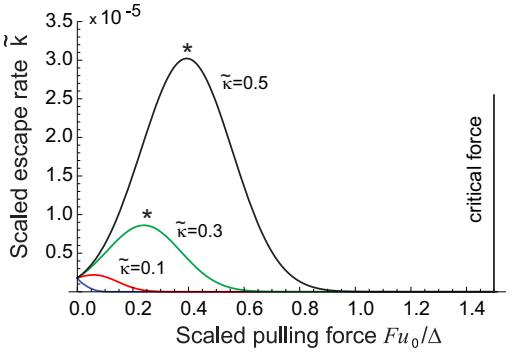

FIGURE 5 The scaled rate of latent complex rupture (and active TGF-β escape), $\tilde{k}$, plotted as function of the applied pulling force (also scaled in nondimensional units, see text). (*Curves*) Different values of substrate stiffness, $\tilde{\kappa} = \kappa u_0^2/\Delta$, labeled on the plot (*lowest curve*, barely visible at low forces, is for $\tilde{\kappa} = 0.02$). On a stiffer substrate, there is a continuous increase in the escape rate of TGF-β as the cell applies more force, until a homeostatic point F^* is reached (the maximum of $\kappa(F)$). Beyond that point, the further increase of forces causes the negative feedback in the free TGF-β release. On soft substrates, only a correspondingly weak pulling force elicits any response from the mechanosensing complex, with only the negative feedback. To see this figure in color, go online.

value, given by $\kappa^* \approx F^2/k_B T$, that is, both the crossover stiffness and the plateau value of the release rate are strong functions of the pulling force the cell exerts at this instance. When $\kappa < \kappa^*$, small changes in stiffness will cause large changes in the TGF-β release rate providing a positive feedback loop to further increase the α-SMA, and ultimately, the strength of the pulling force. Above this value of stiffness, the sensors are telling the cell: "the substrate is as stiff as I can measure at the level of force I can offer." When the force is very small, most substrates will appear as stiff: the cell is working in the saturated part of the curve $k(\kappa)$ with a weak feedback loop. On the other hand, if the pulling force is high to begin with, then very soft substrates offer no resistance and no TGF-β is released to remodel the cell.

So one could trace gradual evolution of a cell after its first deposition onto a substrate from solution. Initially the cell applies a small pulling force F and, unless the substrate is extremely soft (i.e., even at this initial force, $\kappa < \kappa^*$, when no response would follow), the rate of latent complex breaking takes an almost constant value $\tilde{k} \approx 0.4$ (see the *lowest curve* in Fig. 4). As the released TGF-β gets absorbed on the cell surface, more α-SMA is produced, stress fibers start to form, and the pulling force F increases. This further increases the rate of TGF-β release, which is what experiments report.

The same process is presented from a different perspective in Fig. 5, where the rate of latent complex breaking is plotted for a given substrate (fixed κ) against the increasing force F. Apart from the case of very weak substrate, the rate grows as the cell remodels itself to increase the pulling force, until a maximum is reached. A further increase of force results in the negative feedback, which settles the cell evolution at homeostasis (a position labeled by an *asterisk* in Figs. 5 and 6). The stiffer the substrate, the higher the level of free TGF-β and, accordingly, the amount of α-SMA stress fibers one would find in this adjusted cell. Fig. 6 focuses on the region of higher stiffness, where we find that the homeostatic point eventually disappears, replaced by the monotonic increase of the rupture rate with the applied force, all the way until the critical point $F_C = 3\Delta/2u_0$.

THE WEAK FORCE APPROXIMATION

It is important to estimate the actual values of forces and energies involved. Although such an estimate is inevitably

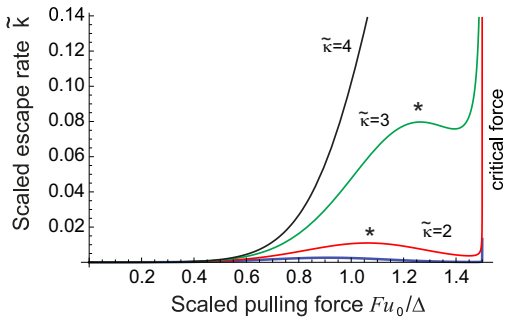

FIGURE 6 The scaled rate of escape as function of the scaled applied pulling force (the same plot as Fig. 5) for a more stiff substrate. The values of $\tilde{\kappa}$ and the position of homeostasis (F^*) are labeled on the plot (*lowest barely visible curve* is for $\tilde{\kappa} = 1$). On a very stiff substrate, $\tilde{\kappa}$>3, there is a continuous increase in the escape rate of TGF-β as the cell applies more force with no homeostatic point F^* (the maximum of $k(F)$) present: there is no region of negative feedback in the free TGF-β release. The critical force limit $F = F_C$ is at $\tilde{f} = 3/2$, at which point the latent complex is ruptured directly. To see this figure in color, go online.

very inaccurate, depending on many individual factors of particular cells and conditions, the order-of-magnitude predictions have to be meaningful. Taking the characteristic energy scale of the latent complex $\Delta = 10$ kcal/mol, the binding energy of a few hydrogen bonds, 10–16 kcal/mol quoted by Hummer and Szabo (29), and the distance needed to distort it to achieve rupture $u_0 = 0.3$ nm (the size of a typical amino-acid monomer), we find the critical force $F_C = 350$ pN. This is a high force unlikely to be generated by a single stress fiber of a cell. For comparison, the force to unfold integrin is quoted as 165 pN (21). Buscemi et al. (21) also quoted 40 pN as the force specifically required to unfold the latent complex of TGF-β1, although this is not purely a dynamic issue and at different times the unfolding would occur at different forces. Other reports investigate the force required to disrupt the fibronectin-integrin-cytoskeleton linkage, finding the value of 1–2 pN (30,31). Various reports (14–16) have measured the actual pulling force F exerted by different cells and in various circumstances, and on very different substrates, nevertheless all converging on values between a few to a few tens of pN (for which see a summary review (32)); note that a single myosin motor exerts ~3 pN of force (33).

Note as well that an increasing body of experimental work finds (by using several ingenious techniques) that cells actually exert much greater overall forces on the substrate features. For instance, individual vascular smooth muscle cells, endothelial cells, and fibroblasts exerted as much as 75 nN of force (34), and forces at the edge of a sheet of epithelial cells were ~12 nN, and ~5 nN underneath the sheet (35). Lecuit et al. (31) specifically report that focal adhesions a few micrometers long can bear forces up to 100 nN. This suggests to us that these high values of force refer to the large assembled (collective) constructions, whereas our interest here is a single molecular adhesion complex, with pN-level forces. We can expect a weak force at first, evolving to perhaps a much greater force on a stiff substrate when larger focal adhesions assemble, but this would serve as a reference point. For $F = 10$ pN, the scaled nondimensional parameter used in plotting is $\tilde{f} = Fu_0/\Delta \sim 0.04$.

If a half-space occupied by an elastic medium (e.g., gel substrate) of the Young modulus E is pulled along the free surface by a point force, another classical problem of Lord Kelvin (36), the response coefficient (spring constant) that we called the stiffness κ is given by $\kappa = (4/3)\pi E\xi$, where ξ is a short-distance cutoff: essentially the size of a microscopic object in the gel that the force is applied to. This sort of relation has been quoted by many authors; e.g., see the review (37) on surface forces in soft polymers. The only relevant length scale in our case (see Fig. 1) is the size of the attachment protein segment, which happens to be the same as a characteristic mesh size of a gel network, with an order-of-magnitude estimate of $\xi \sim 10$ nm. For a very weak gel with $E = 10$ kPa this gives the effective spring constant $\kappa = 4.2 \times 10^{-4}$ N/m and the nondimensional parameter $\tilde{\kappa} = \kappa u_0^2/\Delta \sim 5 \times 10^{-4}$. On stiff glass with $E = 10$ GPa, producing $\tilde{\kappa} \sim 500$, so the whole spectrum of values is explored in a typical experiment.

From the estimates made above, however crude and generic they might be, it is clear that we can safely explore the limit of weak pulling force, $F/F_C << 1$. This allows writing down much simplified analytical expressions and exposes the relevant factors contributing to the rate of breaking of latent TGF-β complex on soft thermally fluctuating substrates. This rate, expressed as $k = J/N_A$ with the parts separately given in Eqs. 6 and 7 (see the Supporting Material for more detail), takes the approximate form of

$$k \approx \frac{9\tilde{D}\Delta}{2\sqrt{2\pi k_B T u_0^3}}\left[1 + \tilde{f}\left(\beta\Delta - \frac{1}{\tilde{\kappa}}\right)\right] e^{-\beta\Delta} e^{-\beta\Delta\frac{\tilde{f}^2}{2\tilde{\kappa}}}, \qquad (8)$$

where $\beta\Delta$ is a shorthand for the ratio (Δ/k_BT), and the nondimensional combinations $\tilde{f}$ and $\tilde{\kappa}$, measuring the force and the stiffness, respectively, have been defined above. At vanishing pulling force, $F \to 0$, this expression reduces to a classical thermal activation rate, $k(0) \propto e^{-\beta\Delta}$, and the ratio $\beta\Delta$ has to be large for the latent complex not to fall apart spontaneously. Indeed the estimates above suggest that $\beta\Delta \sim 16$. The factor in square brackets in Eq. 8 is the remainder of the Bell formula in the weak force approximation: if we ignore the soft substrate and take $\kappa \to \infty$, then this factor reduces to $\exp[Fu_0/k_BT]$. However, we now see that on a soft substrate the pulling force has a very different effect. By carefully analyzing the behavior of the function $k(F,\kappa)$ in different regimes of its parameters, we finally arrive at an interpolating expression that is very accurate in the weak force limit, and is almost exact in the limit of low stiffness—yet remains practical and easy to manipulate. Here we present it in proper dimensional form, instead of using scaled $\tilde{f}$ and $\tilde{\kappa}$:

$$k \approx \frac{9\tilde{D}\Delta}{2\sqrt{2\pi k_B T u_0^3}} \exp\left[-\frac{\Delta - Fu_0}{k_BT} - \frac{F}{\kappa u_0} - \frac{F^2}{2\kappa k_BT}\right]. \qquad (9)$$

Equation 9 is the main analytical result of this article. We remind that the effective stiffness parameter κ is linearly proportional to the Young modulus of the substrate gel. From here we can quickly estimate the substrate stiffness, below which the mechanosensing feedback is always negative (the *low curve* in Fig. 5) and thus we must assume the cell rejects the substrate of excessive softness and detaches from it: this negative slope of $k(F)$ at $F \to 0$ begins at $\tilde{\kappa}_{\min} \le k_BT/\Delta$, or in proper dimensional units: $\kappa_{\min} \le k_BT/u_0^2$. This critical stiffness value is purely determined by the level of thermal noise in the substrate. The other important threshold is the stiffness of a substrate, above which there is no longer a homeostatic point, i.e., the increase of the rate of escape $k(F)$ becomes monotonic (see Fig. 6). The point of $\tilde{\kappa} \approx 3$ corresponds to $\kappa = 0.02$ N/m, and that occurs at the

Young modulus of $E \approx 0.6$ MPa. This is a modulus of a typical tough rubber, so one can see that the cell mechanosensing response on a solid substrate (including the bone, where the modulus measures in GPa range) should be completely different from the response on soft gels (including muscle or even brain tissue).

Equations 8 and 9, although a strong approximation, allow us to analytically describe homeostasis on soft substrates. This is a very important point, because here the cell remodeling in response to the TGF-β mechanosensing signaling should stop: any further increase of free TGF-β, the resulting production of α-SMA, and the increase of the pulling force will cause negative feedback and return the cell to this homeostasis position. The pulling force at this point is easily obtained by finding the maximum of $k(F)$ in Eq. 9, although we must be aware that this is only a qualitative estimate—the full solution for a maximum of $k(F) = J/N_A$ is cumbersome and best studied numerically; in proper dimensional units we have

$$F^* = \frac{k_B T}{u_0}\left(\frac{\kappa u_0^2}{k_B T} - 1\right), \tag{10}$$

where we could employ $\kappa/\kappa_{\min}$ as a shorthand for the ratio $\kappa u_0^2/k_B T$, which essentially compares the elastic and the thermal energy scales in the substrate (instead of the earlier used $\tilde{\kappa} = \kappa u_0^2/\Delta$ that compares the elasticity of substrate and the latent complex). Again we see that thermal fluctuations, represented by the energy factor $k_B T$, are at the core of mechanosensing homeostasis. Therefore, with our chosen parameters (for TGF-β mechanism in (myo)fibroplasts and smooth muscle cells) the homeostasis exists between $\kappa_{\min}$ and $\kappa_{\max} \approx 28\ \kappa_{\min}$, at which point $F^* \geq F_C$. That is, for stiff substrates with a Young modulus $E > 30$ MPa, the cell will no longer be able to achieve homeostasis and will continue to produce stress fibers to increase its pulling force. We might speculate that this is a point of coronary disease onset when the smooth muscle cells in the arterial wall detect a stiff cholesterol plaque underneath. The much lower range of homeostatic substrate stiffness for the neurons and the higher homeostatic range for osteoblasts arise because of a different value of lock stiffness Δ (using a different variant of TGF-β or even a different latent complex altogether) and a different value of lock deformation threshold u_0.

One must be conscious that the theoretical model developed here simplifies many complicated factors and overlooks many details, only focusing on the essential mechanism. Our aim was not to achieve quantitative accuracy, which requires a much more careful input from the biological model, in particular, into the form of the lock potential $U(x)$ and the way the protein binds to the gel substrate (which determines κ)—but to offer an internally self-consistent and mathematically noncontroversial model of mechanosensitivity to replace the earlier more vague ideas.

CONCLUSIONS

This work was inspired by a critical question about one of the most fundamental interactions within living organisms. When trying to explain the mechanical interactions of cells with their environments, an apparent paradox is encountered in the impossibility of measuring stiffness by a probe without a reference point. An extensive literature on this subject carefully sidestepped this issue. Our work shows that even a simple model for a biomolecular mechanosensor can overcome this paradox by using the Brownian motion in the substrate as the reference reservoir: the answer lies in stochastic forces prominent in biomolecular systems. The sensor has evolved in such a way that it is extremely sensitive to the thermally fluctuating behavior of its environment and is able to extract useful information from it. Different substrate stiffness changes not only the equilibrium configuration of the mechanosensor, but also various features in its characteristic potential landscape.

The proposed model for a biomolecular mechanosensor is a likely candidate for several similar sensors. We have described the system as a sensor under constant tension force in series with a viscoelastic substrate, where signaling occurs via a change in the sensor's configuration. We derived an analytical expression for the expected rate of rupture of the latent complex as a function of applied force and substrate elasticity. The final expression for $k(F,\kappa)$ provides convincing behavior in all regimes. It gives the experimentally observed dependence on the substrate stiffness κ: a higher rate of signaling with increasing κ, with a highly nonlinear dependence with clear biological advantages. It also shows that the κ-dependence may be broken down in two distinct regimes, of an extreme sensitivity to stiffness and of saturation and weak κ dependence, with the crossover point dependent on the magnitude of pulling force F: another aspect that matches experimental observation and physical intuition. The expression for the rate also shows a qualitatively satisfactory dependence on F. The rate of signaling increases with F, as the potential barrier to be overcome is lowered—finds a point of homeostasis that the cell attempts to return to from both directions—and then steeply rises to infinity as the external force increases much further toward the critical point, for which the barrier is destroyed and both the model and the latent complex break down. The expression finally obtained reduces to the Bell solution in the high barrier limit—a sanity-check result which matches many simple experiments.

The model developed here builds on and improves related work in the literature, yet it is the first one, to our knowledge, to use analytical stochastic methods of solution applied to the problem of mechanosensitivity. It extends the model proposed by Dudko et al. (13) in a different context to incorporate a substrate with separate mechanical and stochastic characteristics, and shows the correct behavior in the vicinity of the critical force.

In recent years, among the large literature on this subject of mechanical forces felt and exerted by cells, there has been a suggestion that perhaps it is not the constant force, but a fixed deformation of the substrate that cells feel (38,39). We find this concept difficult to reconcile with what we understand about the action of myosin motors on cytoskeleton and the mechanical force balance in quasi-equilibrium the adhesion point must be in. There are other experiments that specifically state that the contractile force generated by the fibroblasts was independent of the stiffness of the resistance (40), and we wish to side with this view.

One can see the analogy of the proposed stochastic mechanism for the change in breaking rate of the TGF-β latent complex on soft substrates with the principle of the enzymatic action (41). The accelerated rate of reaction is achieved by an enzyme localizing the reacting particle near the site (via positional and rotational constraints). In our case, for any given force F from the cell, the localization in the potential well (A) is more pronounced—and so the rate of escape over the barrier increased (even though the height of the barrier itself, ΔV, is not actually changed). In contrast, on a soft substrate, a shallower potential well results in a lower confinement, and correspondingly—a lower rate of the latent complex breaking. One may say that the thermal motion is more readily transferred into a random motion of the attachment point in a soft substrate, and so makes a lesser contribution to the dissociation process.

Further work on this system could include a generalization of the rate expression to a more complex and realistic form for the latent complex potential. It would also be interesting to explore how numerical values obtained by substituting typical cellular pulling forces and distances compare with experiment: we used a very generic set of values although there are no doubt many variations in specific cases.

SUPPORTING MATERIAL

Three figures and 19 equations are available at http://www.biophysj.org/biophysj/supplemental/S0006-3495(13)04218-5.

We are grateful for many useful discussions with K. Franze, B. Hinz, U. Schwarz, and S. Sinha.

This work was funded by the Sims Scholarship, the Cambridge Trusts, and the University of Sydney.

REFERENCES

1. Sinha, S., M. Hoofnagle, …, G. Owens. 2004. Transforming growth factor-β1 signaling contributes to development of smooth muscle cells from embryonic stem cells. *Am. J. Physiol. Cell Physiol.* 287:C1560–C1568.
2. Solon, J., I. Levental, …, P. Janmey. 2007. Fibroblast adaptation and stiffness matching to soft elastic substrates. *Biophys. J.* 93:4453–4461.
3. Yeung, T., P. Georges, …, P. Janmey. 2005. Effects of substrate stiffness on cell morphology, cytoskeletal structure, and adhesion. *Cell Motil. Cytoskeleton.* 60:24–34.
4. Pelham, R., and Y.-L. Wang. 1997. Cell locomotion and focal adhesions are regulated by substrate flexibility. *Proc. Natl. Acad. Sci. USA.* 94:13661–13665.
5. Ghibaudo, M., A. Saez, …, B. Ladoux. 2008. Traction forces and rigidity sensing regulate cell functions. *Soft Matter.* 4:1836–1843.
6. Engler, A., S. Sen, …, D. Discher. 2006. Matrix elasticity directs stem cell lineage specification. *Cell.* 126:677–689.
7. Wipff, P., D. Rifkin, …, B. Hinz. 2007. Myofibroblast contraction activates latent TGF-β1 from the extracellular matrix. *J. Cell Biol.* 179:1311–1323.
8. Sinha, S., A. Heagerty, …, C. Kielty. 2002. Expression of latent TGF-β binding proteins and association with TGF-β1 and fibrillin-1 following arterial injury. *Cardiovasc. Res.* 53:971–983.
9. Cheung, C., A. Bernardo, …, S. Sinha. 2012. Generation of human vascular smooth muscle subtypes provides insight into embryological origin-dependent disease susceptibility. *Nat. Biotechnol.* 15:165–173.
10. Schwarz, U., T. Erdmann, and I. Bischofs. 2006. Focal adhesions as mechanosensors: the two-spring model. *Biosystems.* 83:225–232.
11. Bell, G. 1978. Models for the specific adhesion of cells to cells. *Science.* 200:618–627.
12. Kramers, H. 1940. Brownian motion in a field of force and the diffusion model of chemical reactions. *Physica.* 7:284–304.
13. Dudko, O. K., G. Hummer, and A. Szabo. 2006. Intrinsic rates and activation free energies from single-molecule pulling experiments. *Phys. Rev. Lett.* 96:108101.
14. Dembo, M., and Y. Wang. 1999. Stresses at the cell-to-substrate interface during locomotion of fibroblasts. *Biophys. J.* 76:2307–2316.
15. Schwarz, U., D. Balaban, …, S. Safran. 2002. Calculation of forces at focal adhesions from elastic substrate. *Biophys. J.* 83:1380–1394.
16. Tan, J., J. Tien, …, C. Chen. 2003. Cells lying on a bed of microneedles: an approach to isolate mechanical force. *Proc. Natl. Acad. Sci. USA.* 100:1484–1489.
17. Tomasek, J., G. Gabbiani, …, R. Brown. 2002. Myofibroblasts and mechano-regulation of connective tissue remodeling. *Nat. Rev. Mol. Cell Biol.* 3:349–363.
18. Hinz, B. 2007. Formation and function of the myofibroblast during tissue repair. *J. Invest. Dermatol.* 127:526–537.
19. Arora, P., N. Narani, and C. McCulloch. 1999. The compliance of collagen gels regulates transforming growth factor-β induction of α-smooth muscle actin in fibroblasts. *Am. J. Pathol.* 154:871–182.
20. Hinz, B., G. Celetta, …, C. Chaponnier. 2001. Alpha-smooth muscle actin expression upregulates fibroblast contractile activity. *Mol. Biol. Cell.* 12:2730–2741.
21. Buscemi, L., D. Ramonet, …, B. Hinz. 2011. The single-molecule mechanics of the latent TGF-β1 complex. *Curr. Biol.* 21:2046–2054.
22. Wells, P., and D. Discher. 2008. Matrix elasticity, cytoskeletal tension, and TGF-β: the insoluble and soluble meet. *Sci. Signal.* 1:1–3.
23. Graham, R. 1977. Covariant formulation of non-equilibrium statistical thermodynamics. *Zeit. Phys. B.* 26:397–405.
24. Chandrasekhar, S. 1943. Stochastic problems in physics and astronomy. *Rev. Mod. Phys.* 15:1–89.
25. Hänggi, P., P. Talkner, and M. Borkovec. 1990. Reaction rate theories: 50 years after Kramers. *Rev. Mod. Phys.* 62:251–340.
26. Yohichi, S., and O. K. Dudko. 2010. Single-molecule rupture dynamics on multidimensional landscapes. *Phys. Rev. Lett.* 104:048101.
27. Berezhkovskii, A. M., V. Y. Zitserman, and A. Polimeno. 1996. Numerical test of Kramers reaction rate theory in two dimensions. *J. Chem. Phys.* 105:6342–6357.
28. Langer, J. S. 1969. Statistical theory of the decay of metastable states. *Ann. Phys.* 54:258–275.
29. Hummer, G., and A. Szabo. 2003. Kinetics from nonequilibrium single-molecule pulling experiments. *Biophys. J.* 85:5–15.

30. Brenner, M. D., R. Zhou, and T. Ha. 2011. Forcing a connection: impacts of single-molecule force spectroscopy on in vivo tension sensing. *Biopolymers.* 95:332–344.

31. Lecuit, T., P. F. Lenne, and E. Munro. 2011. Force generation, transmission, and integration during cell and tissue morphogenesis. *Annu. Rev. Cell Dev. Biol.* 27:157–184.

32. Bershadsky, A. D., N. Q. Balaban, and B. Geiger. 2003. Adhesion-dependent cell mechanosensitivity. *Annu. Rev. Cell Dev. Biol.* 19:677–695.

33. Finer, J. T., R. M. Simmons, and J. A. Spudich. 1994. Single myosin molecular mechanics: picoNewton forces and nanometer steps. *Nature.* 368:113–119.

34. Ingber, D. E. 2003. Mechanosensation through integrins: cells act locally but think globally. *Proc. Natl. Acad. Sci. USA.* 100:1472–1474.

35. Saez, A., E. Anon, …, B. Ladoux. 2010. Traction forces exerted by epithelial cell sheets. *J. Phys. Cond. Mat.* 22:194119.

36. Landau, L. D., and I. M. Lifshitz. 1986. Theory of Elasticity, 3rd Ed. Butterworth-Heinemann, Oxford, UK.

37. Cappella, B., and G. Dietler. 1999. Force-distance curves by atomic force microscopy. *Surf. Sci. Rep.* 34:1–104.

38. Saez, A., A. Buguin, …, B. Ladoux. 2005. Is the mechanical activity of epithelial cells controlled by deformations or forces? *Biophys. J.* 89:L52–L54.

39. De, R., A. Zemel, and S. A. Safran. 2008. Do cells sense stress or strain? Measurement of cellular orientation can provide a clue. *Biophys. J.* 94:L29–L31.

40. Freyman, T. M., I. V. Yannas, …, L. J. Gibson. 2002. Fibroblast contractile force is independent of the stiffness which resists the contraction. *Exp. Cell Res.* 272:153–162.

41. Jackson, M. B. 2006. Molecular and Cellular Biophysics. Cambridge University Press, Cambridge, UK.

Supplementary Information

"How cells feel: stochastic model for a molecular mechanosensor"

Matteo Escudé, Michelle K. Rigozzi and Eugene M. Terentjev*

E-mail: emt1000@cam.ac.uk

Figure 1 reminds the reader about the construction of the model. The pictorial of the sequence of elements in the adhesion center illustrates the idea of how the TGF-β signal might be sent to the cell, but it also highlights the 'paradox'. On the short timescales of Brownian motion, at which the 'decision' about breaking or preserving the latent complex is made, there is no coherent motion in the overdamped macromolecular system – and therefore the force F is transmitted along the whole series of elements. This means that, whether the soft substrate deforms by this pulling force (as shown in the picture) or a stiffer substrate stays in its original position, the force acting on the latent complex is always F – and there could be no sensitivity to the degree of the above deformation (which is indeed measured by the stiffness κ).

The scheme in the right panel of Figure 1 illustrates the mechanical elements. Again, on a much longer time scales both the cell and the substrate may experience creep (irreversible deformation). However, on the time scales relevant to our problem, that is, when the Kramers-like 'escape' over the potential barrier $U(x)$ signifies the spontaneous breaking of the latent complex and the release of signalling TGF-β, both elements are elastic – in the sense that they each have a fixed equilibrium value of deformation induced by an external force. Of course, both elements must also have the energy dissipation (friction) mechanism to balance the energy input from the thermal motion (fluctuation-dissipation theorem), which is expressed by the friction constants γ_1 and γ_2.

*To whom correspondence should be addressed

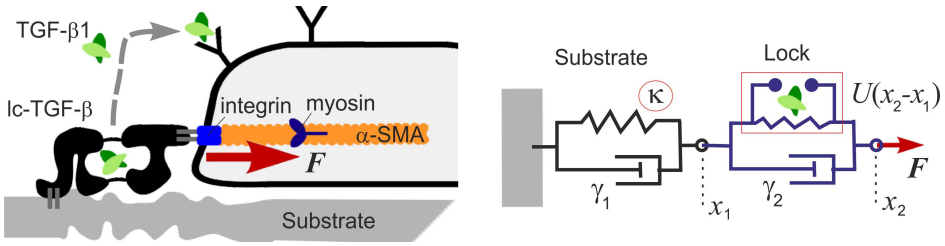

Figure 1: The reminder of the key points of the model: [left] the qualitative explanation for the release of active TGF-β signalling to the cell about the properties of the substrate; [right] the series of Voigt-like models describing the substrate (stiffness κ, friction constant γ_1 displacement of the binding point x_1) and the latent complex with the friction γ_2 and displacement x_2 controlled by the "lock" potential $U(x_2-x_1)$.

Equations (1) and (2) of the main paper express the Langevin dynamics of these two elements in series, as measured at the points measured by x_1 and x_2.

There are several ways of converting the microscopic stochastic problem described by Langevin dynamics into the kinetic equation(s) for the probability distributions. We follow the method summarized by Graham, which starts by expressing the Langevin equations for independent variables $q_\nu(t)$ in the 'standard' form:

$$\dot{q}_\nu = f_\nu(q) + g^i_\nu(q)\zeta_i(t), \tag{1}$$

where $f_\nu(q)$ are the corresponding dynamic forces and $\zeta_i(t)$ the stochastic force normalized to unity: $\langle \zeta_i(t)\zeta_j(t')\rangle = \delta_{ij}\delta(t-t')$ so that the actual intensity of the relevant stochastic force is expressed by a coefficient $g^i_\nu(q)$. In our case, for the two fluctuating variables $x_1(t)$ and $x_2(t)$ these parameters are quite simple:

$$f_1(x_1,x_2) = \frac{1}{\gamma_1}\left[-\kappa x_1 + \frac{\mathrm{d}U}{\mathrm{d}(x_2-x_1)}\right], \qquad f_2(x_1,x_2) = \frac{1}{\gamma_2}\left[-\frac{\mathrm{d}U}{\mathrm{d}(x_2-x_1)} + F\right]; \tag{2}$$

$$g_1 = \sqrt{2k_BT/\gamma_1}, \qquad g_2 = \sqrt{2k_BT/\gamma_2}. \tag{3}$$

Remaining in the overdamped limit (i.e. at timescales much greater than the characteristic relaxation time m/γ) allows us to dispense with the dependence on the corresponding velocity space in

the full Fokker-Planck formalism, and obtain directly:

$$\frac{\partial P(x_1,x_2,t)}{\partial t} = -\frac{\partial}{\partial x_1}\left[f_1(x_1,x_2)\cdot P\right] - \frac{\partial}{\partial x_2}\left[f_2(x_1,x_2)\cdot P\right] + k_B T\left[\frac{1}{\gamma_1}\frac{\partial^2}{\partial x_1^2} + \frac{1}{\gamma_2}\frac{\partial^2}{\partial x_2^2}\right] P.$$

The corresponding expressions for the diffusion currents take the explicit form:

$$J_1 = \frac{1}{\gamma_1}\left[-\kappa x_1 + \frac{\mathrm{d}U}{\mathrm{d}(x_2-x_1)} - k_B T\frac{\partial}{\partial x_1}\right] P, \qquad J_2 = \frac{1}{\gamma_2}\left[-\frac{\mathrm{d}U}{\mathrm{d}(x_2-x_1)} + F - k_B T\frac{\partial}{\partial x_2}\right] P. \quad (4)$$

In their current form it is not possible to write the components J_1 and J_2 as a single two-dimensional vector, because they are written with nominally different diffusion constants: $k_B T/\gamma_1$ and $k_B T/\gamma_2$. This issue can be overcome by scaling the variables: $x_1 = \sqrt{\gamma_2/\gamma_1}\tilde{x}_1$, $x_2 = \sqrt{\gamma_1/\gamma_2}\tilde{x}_2$. This allows us to write the current in general vector form:

$$\tilde{J}_i = -\frac{k_B T}{\sqrt{\gamma_1\gamma_2}} e^{-\tilde{V}_E/k_B T}\frac{\partial}{\partial \tilde{x}_i}\left(e^{\tilde{V}_E/k_B T} P\right) \qquad i = 1,2\,, \quad (5)$$

with a unique diffusion coefficient $\tilde{D} = k_B T/\sqrt{\gamma_1\gamma_2}$ and an effective potential acting in the plane (x_1,x_2): $V_E(x_1,x_2) = \frac{1}{2}\kappa x_1^2 - F x_2 + U(x_2-x_1)$. This effective potential surface represents the landscape over which the substrate and complex particles move, subject to collisions caused by thermal motion in the medium.

To apply the analysis to a real physical system, it is necessary to express $U(u)$, with the relative stretching of the 'lock' $u = x_2 - x_1$, in a particular functional form. In the 60 years past Kramers original work, many such forms were tried, with a great variety of barrier shapes. It is, however, clear that only two key features of such a potential are relevant: the distance u_0 of the barrier from the position of metastable minimum – and the barrier height Δ; in contrast, the shape of the potential around the minimum and around the barrier only contribute in a minor way to the pre-exponential factors. In recent years it becomes more and more common to use a cubic function that has a simple and explicit representation of the two mentioned key features, and also naturally excludes the possibility of rebinding by falling to negative infinity for large u. The form is adjusted

so that the minimum (point A) is at $u = 0$ and the maximum (point C) at $u = u_0$:

$$U(u) = \frac{3}{2}\Delta\left(\frac{u}{u_0} - \frac{1}{2}\right) - 2\Delta\left(\frac{u}{u_0} - \frac{1}{2}\right)^3 + \frac{\Delta}{2}. \tag{6}$$

When the external force F and the spring potential of the elastic substrate are added in the effective potential $V_E(x_1, u)$, we find that it has two extrema at:

$$x_1^* = \frac{F}{\kappa}, \qquad u_\pm^* = \frac{1}{2}u_0\left(1 \pm \sqrt{1 - \frac{2}{3}\frac{Fu_0}{\Delta}}\right). \tag{7}$$

The solution u_+^* corresponds to the saddle point (i.e. the barrier the systems needs to overcome) and the solution u_-^* marks the minimum of the two-dimensional well; the two extrema have the same x_1 coordinate; for $F_C = 3\Delta/2u_0$ the two extrema coincide so there is no longer any energy barrier to hold the latent complex together. The effective barrier height, Δ_E, is defined as the difference in potential between the minimum of the well and the saddle point: $\Delta_E = \Delta(1 - 2Fu_0/3\Delta)^{\frac{3}{2}}$. This expression, alongside the probability currents, are the starting point for the application of the Kramers theory.

Applying the Kramers theory to generalized multidimensional problems causes several computational problems; for this reason it is usually more convenient to reduce the system to a one-dimensional barrier escape. In our context this means we identify the path taken by the system in the effective potential landscape. We stay close to the original approach of Kramers, but differ in the technique used to evaluate the integrals for the path. Let us make the path dependent on a new single variable, u for convenience, which coincides with the previously defined $u = x_2 - x_1$ when $F = 0$. Starting with the assumption of steady current, we may write for the path A $\rightarrow$ C $\rightarrow$ B:

$$J\int_A^B \frac{\gamma}{k_B T} e^{V_E/k_B T}\,\mathrm{d}u = \left(P e^{V_E/k_B T}\right)\Big|_B^A. \tag{8}$$

Taking the potential at the point to which the particles 'escape' (B) to be such that $V(u_B) \sim -\infty$, which is consistent with the rapidly decreasing cubic describing $U(u)$, the expression for the con-

stant probability current can be simplified:

$$J = \frac{P(u_A)\mathrm{e}^{V_E(u_A)/k_BT}}{\int_A^B \frac{\gamma}{k_BT}\mathrm{e}^{V_E/k_BT}\mathrm{d}u}. \tag{9}$$

Moving $\mathrm{e}^{V_E(u_A)/k_BT}$ from the numerator to the denominator, the integrand of this expression becomes $I(u) = \mathrm{e}^{(V_E(u)-V_E(u_A))/k_BT}$. To approximate the value of this integral the original solution by Kramers uses the method of saddle-point integration, approximating the exponent of the integrand with a second order polynomial. This has been generally followed in the literature since. However, this classical method has a problem in the region of $F \to F_C$, that is, near the point where the barrier disappears and the system has no restriction escaping from its originally metastable state (A). This problem has been known since Kramers himself, and is usually avoided merely by assuming low forces: in the saddle-point method one has to extend the integration region to infinity (which is normally safe, since the Gaussian exponential cuts the integrand to zero far away from the barrier crest). So, although the 'curvature' $V_E''(u_C)$ goes to zero, actually as $\sqrt{F_C - F}$, the error of this saddle-point approximation increases. If one follows the classical recipe literally, it leads to the completely wrong result that $J \to 0$ as $F \to F_C$. Over the years, there were several much more accurate treatments of this problem, but we choose our own (as it seems all these methods are all worth each other: all converging to the classical Kramers result at $F \to 0$, while leading to the diverging flux at $F \to F_C$, in slightly different ways).

Our method is to fit a second order polynomial to the integrand $I(u)$ itself, integrating it from A to C, and then doubling this to approximate the value of the integral from A to B. The chosen polynomial shares its maximum with the maximum $I(u_C)$ and also passes through the minimum $I(u_A)$. The fitting parabola is given by $I(u) \approx -\left(I(u_C) - I(u_A)\right)(u-u_C)^2/(u_C-u_A)^2 + I(u_C)$, which may be substituted in the expression for the integrand:

$$\begin{aligned}\int_A^B \mathrm{e}^{(V(u)-V(u_A))/k_BT}\mathrm{d}u &\approx 2\int_A^C -\frac{\mathrm{e}^{(V(u_C)-V(u_A))/k_BT}-1}{(u_C-u_A)^2}(u-u_C)^2 + \mathrm{e}^{(V(u_C)-V(u_A))/k_BT}\mathrm{d}u \\ &= \frac{2}{3}(u_C-u_A)\left(1+2\mathrm{e}^{(V(u_C)-V(u_A))/k_BT}\right).\end{aligned} \tag{10}$$

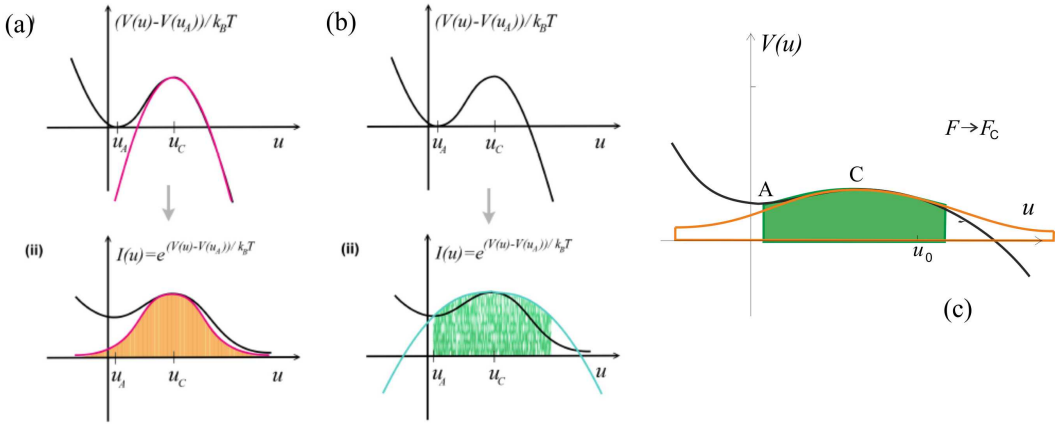

Figure 2: Comparison between the classical saddle-point integration (a) and the method of integration via model parabola used here (b): The exponent of the integrand (a)(i) is approximated by a second-order polynomial (shown in pink). In contrast, the integrand itself (b)(ii) is approximated in the method used here; the chosen second-order function shares the maxima of the integrand at u_C, passes though the functionŠs minima at u_A (shown in green), and the integral is taken over twice the area from u_A to u_C, indicated by the shaded region. (c) The limit of $F \to F_C$ illustrates the difference more explicitly, showing how the integral of the saddle-point approximation diverges, while the approximating by parabola with a fixed integration width gives a plausible result.

Here the distance between the extrema is $(u_C - u_A) = u_0\sqrt{1-2Fu_0/3\Delta}$ and the remaining energy barrier is expressed by $V(u_C) - V(u_A) = \Delta(1-2Fu_0/3\Delta)^{3/2}$ for our chosen potential energy. This expression for the integral in denominator may now be put back to obtain the probability flux:

$$J = \frac{k_B T}{\gamma} P(u_A) \frac{3}{2} \left[(u_C - u_A) \left(1 + 2\mathrm{e}^{(V(u_C)-V(u_A))/k_B T} \right) \right]. \tag{11}$$

The escape rate k is given by the flux J normalized by the numbers of particles in the well at A, ν_A. Quasi-stationary conditions are assumed, requiring the barrier to be large compared to thermal fluctuations ($\Delta \gg k_B T$). We are therefore justified to assume the Maxwell-Boltzmann distribution is valid in the neighborhood of (A), again following the classical Kramers analysis:

$$\mathrm{d}\nu_A = P(u_A)\mathrm{e}^{-V_E/k_B T}\,\mathrm{d}u, \tag{12}$$

which may be integrated to find the number of particles. Approximating the potential about the potential minimum at u_A by a Taylor series to second order, the number of particles may be ap-

proximated to

$$\nu_A = \frac{P(u_A)}{\omega_A}\sqrt{2\pi k_B T}\, \mathrm{e}^{F^2/2\kappa k_B T}, \tag{13}$$

where ω_A is the curvature of the potential well at the minimum (A), while the exponential factor is a reminder that the depth of this minimum is no longer at $V_E = 0$ – which merely expresses the fact that the system states would accumulate more densely in a deeper energy minimum of the stretched substrate. We are now in the position to write down an expression for the ratio of the rate with a force a applied, $k(F)$, to the initial rate with no force, k_0, which frees the expression from constant factors:

$$\frac{k(F)}{k_0} = \frac{\omega_A(F)}{\omega_A(0)}\mathrm{e}^{-F^2/2\kappa k_B T}\,\frac{u_{C0}-u_{A0}}{u_{CF}-u_{AF}}\,\frac{1+2\mathrm{e}^{(V(u_{C0})-V(u_{A0}))/k_B T}}{1+2\mathrm{e}^{(V(u_{CF})-V(u_{AF}))/k_B T}}. \tag{14}$$

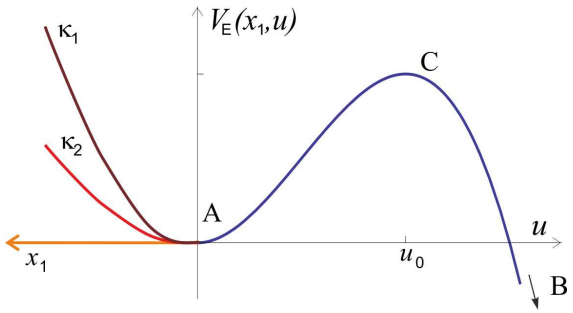

Figure 3: The illustration of a two-sided minimum of the effective potential $V_E(x_1,u)$, with the descent towards the minimum (nearly) along the x_1 direction has the curvature $\omega_{A1} = \sqrt{\kappa}$, while the climb towards the barrier along the u-direction has the curvature ω_{A2} given earlier in the text.

Whilst the positions and values of the potential at the different points are readily calculated from the previously obtained expressions, the curvature term ω_A requires further attention. The curvature we seek to find is composed by a first segment O $\rightarrow$ A and a second segment A $\rightarrow$ C, see Fig.3(b) in the main paper. To first order the curvature of the first segment will be simply $\omega_{A1}^2 = \kappa$, which may be visualized intuitively since, when working with forces safely below the critical, the path follows closely the x_1 axis. The curvature of the path A $\rightarrow$ C, when evaluated at the bottom of the well, may be taken to be equivalent to the modulus of the value of the second derivative of

the potential $U(u)$ at that point:

$$\omega_{A2}^2 = \frac{6\Delta}{u_0^2}\sqrt{1-\frac{2}{3}\frac{Fu_0}{\Delta}}. \tag{15}$$

It is therefore possible to approximate the total curvature ω_A^2 (which controls the result of the integration around u_A) as an average of these two values weighted by distance. That is, the weight of the first curvature will be the distance from O to A (F/κ to first order), while the weight of the second will be the distance from A to C, given above. As a result we obtain:

$$\omega_A^2 = \frac{6\kappa\Delta\left(1-\frac{1}{2}\frac{Fu_0}{\Delta}\right)}{u_0\left(F+\kappa u_0\sqrt{1-\frac{2}{3}\frac{Fu_0}{\Delta}}\right)}. \tag{16}$$

With this last piece in place we may proceed to substituting all the components into $k(F)=\frac{J}{v_A}$ to obtain:

$$k(F) = \frac{9\tilde{D}\Delta}{2\sqrt{2\pi k_B T}u_0^3}\frac{\mathrm{e}^{-F^2/2\kappa k_B T}\sqrt{1-2Fu_0/3\Delta}}{\left(1+2\exp\left[(1-2Fu_0/3\Delta)^{3/2}\Delta/k_BT\right]\right)\left(F/\kappa u_0+\sqrt{1-Fu_0/3\Delta}\right)} \tag{17}$$

As mentioned earlier, it is often considered useful to present the ratio of the breaking rate $k(F)$ and its 'bare' value at zero force. In doing so several constant factors cancel (in particular, the effective diffusion coefficient) and the expression allows the quick examination of the effects of the pulling force:

$$\frac{k(F)}{k_0} = \frac{\mathrm{e}^{-F^2/2\kappa k_B T}\sqrt{1-2Fu_0/3\Delta}\,(1+2\exp\left[\Delta/k_BT\right])}{\left(1+2\exp\left[(1-2Fu_0/3\Delta)^{3/2}\Delta/k_BT\right]\right)}. \tag{18}$$

Examining both expressions we see the natural dimensional parameters measuring the external pulling force relative to the characteristic returning force of the lock (the latent complex): $\tilde{f}=Fu_0/\Delta$, and similarly – the substrate stiffness: $\tilde{\kappa}=\kappa u_0^2/\Delta$. Similarly, the escape rate of the latent complex has its own natural units, making the non-dimensional measure $\tilde{k}=k\cdot 2\sqrt{2\pi k_BT}u_0^3/9\tilde{D}\Delta$. Of course, the non-dimensional ratio Δ/k_BT is the measure how strongly confined the latent complex is, and since there is no (or very little) spontaneous 'leakage' of TGF-β from it, we expect $\Delta/k_BT \gg 1$.

Two simplified expressions are presented and explored in the main text. One is simply the expansion of $k(F)$ in the limit of weak force ($\tilde{f} \ll 1$), however, retaining the key exponential factor $\exp[-F^2/2\kappa k_B T]$. The other expression is 'reconstructed' to interpolate a simple formula into the weak substrate limit ($\tilde{\kappa} \ll 1$) by lifting the linear expressions of the nature $(1-a)$ into the exponential form e^{-a}:

$$k \approx \frac{9\tilde{D}\Delta}{2\sqrt{2\pi k_B T u_0^3}}\, \mathrm{e}^{-(\Delta - F u_0)/k_B T}\, \mathrm{e}^{-F/\kappa u_0}\, \mathrm{e}^{-F^2/2\kappa k_B T}. \tag{19}$$